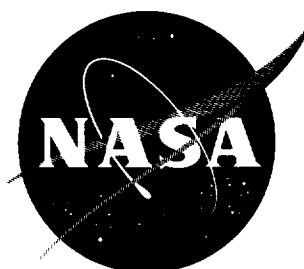NASA TN D-987

NASA

TECHNICAL NOTE

D-987

CROSS-SECTIONAL DEFORMATIONS

OF MONOCOQUE BEAMS AND THEIR EFFECTS ON THE

NATURAL VIBRATION FREQUENCIES

By Robert G. Thomson and Edwin T. Kruszewski

Langley Research Center
Langley Air Force Base, Va.

NATIONAL AERONAUTICS AND SPACE ADMINISTRATION

WASHINGTON   December 1961

.F

L
1
4
4
4

NATIONAL AERONAUTICS AND SPACE ADMINISTRATION

TECHNICAL NOTE D-987

CROSS-SECTIONAL DEFORMATIONS

OF MONOCOQUE BEAMS AND THEIR EFFECTS ON THE

NATURAL VIBRATION FREQUENCIES

By Robert G. Thomson and Edwin T. Kruszewski

SUMMARY

The variational principle, differential equations, and boundary conditions governing the cross-sectional distortions due to inertia loading of a two-dimensional model of a thin monocoque wing are shown. A theoretical analysis of this simplified model is made in order to determine the nature of the coupling between the cross-sectional modes and the spanwise deformation modes. General solutions are obtained in finite-difference form for arbitrary cross sections and an exact solution is presented for a parabolic-arc cross section of constant cover thickness. The application of these results in evaluating the coupled frequencies of the actual structure is discussed. Frequencies evaluated for a parabolic-arc monocoque beam show good agreement with experimental values.

INTRODUCTION

Chordwise modes - that is, modes whose chordwise variation in deflection is such that more than one node line exists at every cross section along the span - have been observed in several dynamic investigations of pure monocoque and multiweb wing models. For example, in an extensive series of tests of aerodynamically heated multiweb wing structures the principal mode of failure was established to be chordwise flutter. (See ref. 1.) Also, in an investigation of the vibrational characteristics of circular-arc monocoque beams, discussed in reference 2, several "extra" resonant conditions were observed experimentally which, although referred to as panel modes, are more accurately described as chordwise or cross-sectional modes. In addition, the results of reference 2 indicate that the accuracy of the predicted overall bending and torsion frequencies, even after the inclusion of important secondary effects, such as transverse shear and shear lag in bending and restraint of warping in torsion, are considerably impaired by the presence of these chordwise modes. For instance, the

calculated frequency of even the first symmetrical torsion mode (mode 2 in table II of ref. 2) differed from the one obtained experimentally by 72 percent while the third symmetrical mode differed by more than 250 percent.

The influence of cross-sectional distortions on the overall beam modes was investigated in references 3 and 4. These investigations, however, were not concerned primarily with the prediction of cross-sectional modes but rather with the influence of cross-sectional flexibilities on the overall beam modes. Furthermore, neither analysis is applicable to monocoque or multiweb wings with thin airfoil-type cross sections such as those used in references 1 and 2.

The purpose of the present paper is to investigate the chordwise modes and frequencies of beams with thin airfoil-type cross sections and to determine the influence of cross-sectional flexibilities on the overall beam frequencies. A simplified model which embodies the principal mechanisms of cross-sectional and sparwise flexibility is analyzed. The differential equations and boundary conditions for the simplified model appropriate for wings of arbitrary airfoil-type cross section are derived. An exact solution is found for the model for the particular case of a monocoque wing of parabolic cross section. In addition, a general solution is presented in finite-difference form by applying the calculus of variations directly to the energy expressions. A discussion is made of the use of these results to predict the frequencies of both the coupled cross-sectional modes and the overall beam modes of a monocoque wing presented in reference 2.

<div align="center">SYMBOLS</div>

c	chord length of beam
E	modulus of elasticity
h	distance from x-axis to median line of skin
h_0	maximum value of h
I	moment of inertia about median line of skin, $t^3/12$
k_1, k_2, k	spring constants
M	moment (see fig. 2)
N	number of discrete stations in finite-difference analysis

$n = 0, 1, 2, \ldots, N$

r	radius of curvature of midplane of beam
s	tangential coordinate
T	maximum kinetic energy
t	skin thickness
U	maximum strain energy
u	displacement of midplane in x-direction
$\bar{u}$	displacement in s-direction, $h'w + u$
V	shear (see fig. 2)
w	deflection in z-direction (positive upward)
$\bar{w}$	deflection normal to s-direction
x	chordwise coordinate
y	spanwise coordinate
z	coordinate perpendicular to x and y coordinates
α	frequency coefficient
α_c	frequency coefficient for uncoupled chordwise mode
ϵ_s	strain in s-direction
ϵ_x	strain in x-direction
η	nondimensional distance between stations on the half-chord
λ	normal midplane force in the beam
$\xi = \dfrac{2x}{c} - 1$	
ρ	mass density of cover
ω	natural frequency
ω_c	uncoupled cross-sectional frequency

$\omega_{c,1}$ fundamental or first uncoupled cross-sectional frequency

ω_{exper} experimental natural frequency

$\omega_{r,B}$ rigid-body bending frequency, $\sqrt{\dfrac{k}{c\rho t}}$

$\omega_{r,T}$ rigid-body torsion frequency, $\sqrt{\dfrac{3k}{c\rho t}}$

Primes on symbols denote differentiation with respect to x; primes on matrices denote the transpose of a matrix.

THEORETICAL ANALYSIS

Idealization

A rigorous approach to the problem of the vibrational characteristics of a monocoque wing which includes both spanwise and cross-sectional flexibilities would, of necessity, involve some type of shell analysis. A more appealing although less rigorous approach, however, is to investigate first the uncoupled chordwise and spanwise characteristics of the structure independently and then determine the influence on the natural frequencies of the coupling of these motions. This can be done in a manner similar to that used in references 3 and 4 by mounting a typical cross section of the wing on elastic supports in such a way as to allow for the necessary overall degrees of freedom.

The only structures considered in this paper have uniform properties in the spanwise direction with a symmetrical curved airfoil cross section, as shown in figure l(a). The wing or beam is of either pure monocoque or multiweb construction with no, or relatively few, bulkheads. An idealized structure that can be easily analyzed but still possesses essentially the same cross-sectional and spanwise flexibilities as the original is shown in figure l(b).

The idealized structure consists of two curved beams attached at the ends to elastic supports in such a manner as to maintain the angle between the beams at each end. The idealization is the same for both the monocoque and multiweb prototypes. Consequently, the spanwise webs of the multiweb structure are assumed to contribute nothing to the chordwise stiffness of the wing. The webs, however, do tend to prevent any relative motion between the top and bottom covers. Hence the additional assumption is made that deflections of the top and bottom beams in the idealized structure are the same. The depth of the individual beams in

the idealized structure is taken to be the same as the thickness of the covers in the prototype. The stiffness of the elastic supports or springs is chosen to duplicate the bending or torsional stiffness of the prototype, depending on whether the motion is symmetrical or antisymmetrical about the midchord.

Method of Analysis

The structure to be analyzed is shown in figure 2 along with the coordinate system and sign convention to be used. As the structure is symmetrical about the x-axis and the distance between the top and bottom segments is maintained, only half of the structure need be considered. Each segment is assumed to carry midplane forces in addition to transverse shear and bending moments (see fig. 2), and will be considered to act in a manner consistent with elementary beam theory (i.e., plane sections remain plane).

The strain in the midplane of the beam is given by

$$\epsilon_s = \frac{\bar{w}}{r} + \frac{d\bar{u}}{ds} \tag{1}$$

where

$\bar{w}$ deflection normal to s-direction

r radius of curvature of midplane

$\bar{u}$ displacement in s-direction

s tangential coordinate

Since the cross section of the prototype being analyzed is that of a thin airfoil section and deformations are considered small, the tangential coordinate s can be approximated by the chordwise coordinate x, and the curvature by $-h''$. Furthermore, the deflection $\bar{w}$ can be considered to be the same as the deflection in the z-direction, and the displacement in the s-direction can be written as

$$\bar{u} = h'w + u \tag{2}$$

where w is the deflection in the z-direction and u is the displacement in the x-direction. Hence the expression for strain in equation (1) becomes

$$\epsilon_x = h'w' + u' \tag{3}$$

If this expression is used for the strain, and w and u are considered as amplitudes of displacement, the maximum strain energy for one of the covers of the idealized structure vibrating in a natural mode becomes

$$U = \frac{1}{2} \int_0^c EI(w'')^2 dx + \int_0^c \lambda(h'w' + u')dx + \frac{1}{4} k_1 w^2(c) + \frac{1}{4} k_2 w^2(0) \quad (4)$$

where

EI   bending stiffness of beam

λ normal midplane force

k_1, k_2 spring constants

The first term in equation (4) represents the contribution to the strain energy due to bending of the idealized structure, the second represents the strain energy due to the midplane force, and the third and fourth terms are the potential energy of the spring mounts.

In the present analysis the force λ will be considered constant and equal to the average midplane force; hence, with the use of equation (3),

$$\lambda = \frac{1}{c} \int_0^c Et(h'w' + u')dx \quad (5)$$

Furthermore, if inextensional theory is assumed u' vanishes in equation (4), and equation (5) becomes

$$\lambda = \frac{1}{c} \int_0^c Eth'w'dx \quad (6)$$

The maximum kinetic energy of the idealized structure vibrating in a natural mode is

$$T = \frac{1}{2} \int_0^c \rho t \omega^2 w^2 dx \quad (7)$$

where ω is the natural circular frequency of the mode under consideration and ρ is the mass density of the cover.

A natural mode of vibration must satisfy the variational equation

$$\delta(U - T) = 0 \qquad (8)$$

where the variation is taken independently with respect to w . Application of equation (8) and the usual methods of the calculus of variations results in the following differential equation and boundary conditions:

$$(EIw'')'' - \lambda h'' - \rho t\omega^2 w = 0 \qquad (9)$$

$$(EIw'')\delta w' \Big|_{x=c} = 0 \qquad (10)$$

$$\left[(EIw'')' - \lambda h' - \frac{k_1}{2} w\right]\delta w \Big|_{x=c} = 0 \qquad (11)$$

$$(EIw'')\delta w' \Big|_{x=0} = 0 \qquad (12)$$

$$\left[(EIw'')' - \lambda h' + \frac{k_2}{2} w\right]\delta w \Big|_{x=0} = 0 \qquad (13)$$

where λ is given by equation (6).

If the cover thicknesses of the original wing are constant and if the half-depth h of the wing is approximately parabolic (as, for example, the circular-arc airfoils used in refs. 1 and 2) an exact solution to the differential equation is possible and is discussed in the next section. However, for an airfoil of arbitrary shape and variable cover thickness it is unlikely that an exact solution can be found. For these cases the use of some approximate variational procedure is advisable. One such approach is presented in the appendix. Here, by a procedure similar to that discussed in reference 5, the energy is expressed in matrix form in terms of the deflections at discrete points by means of finite-difference relationships. The variational procedure results in a frequency equation in matrix form from which the mode shapes and frequencies of the structure can be calculated.

Exact Solution of Idealization of the Monocoque Beam

of Parabolic-Arc Cross Section

For an airfoil of doubly symmetrical cross section and constant cover thickness whose half-depth h can be represented by a parabolic equation, an exact solution to the differential equation for the cross section mounted on springs is possible. In order to take advantage of

the double symmetry the origin of the coordinate system is now relocated at the midchord of the cross section and the nondimensional coordinate $\xi = \frac{2x}{c} - 1$ is used. Thus, the half-depth can be represented as

$$h = h_0\left(1 - \xi^2\right) \qquad (14)$$

Furthermore, the spring constants are identical, so that $k_1 = k_2 = k$.

Equation (9) can now be written in nondimensional form as

$$\frac{d^4w}{d\xi^4} - \frac{\lambda c^2}{4EI}\frac{d^2h}{d\xi^2} - \alpha^4 w = 0 \qquad (15)$$

where

$$\alpha^4 = \frac{c^4 \rho t \omega^2}{16EI} \qquad (16)$$

$$\lambda = \frac{4h_0 tE}{c^2}\left[w(-1) - w(1) + \int_{-1}^{1} w(\xi)d\xi\right] \qquad (17)$$

Because of the constant cover thicknesses of the original wing, the more stringent conditions of inextensional theory are not necessary in determining λ. It need only be assumed that there is no overall short-ening or stretching of the cross section; then the integral of u' will vanish in equations (4) and (5) instead of u' being zero everywhere.

Because, in the general solution to the differential equation, the symmetrical and antisymmetrical parts are easily recognizable, they are presented separately.

Symmetrical solution.- For the symmetrical solution the boundary conditions, as given by equations (10) and (11), can be written in non-dimensional form as

$$\left.\frac{d^2w}{d\xi^2}\right|_{\xi=1} = 0 \qquad (18)$$

and

$$\left(\frac{2}{c}\right)^3 EI\frac{d^3w}{d\xi^3} + \frac{4h_0\lambda}{c}\xi - \frac{k}{2}w\bigg|_{\xi=1} = 0 \qquad (19)$$

The symmetrical solution to the homogeneous part of equation (15) is

$$w = A_1 \cos \alpha\xi + B_1 \cosh \alpha\xi \tag{20}$$

and the particular solution is simply

$$w = \frac{\lambda h_o c^2}{2EI\alpha^4} \tag{21}$$

Thus

$$w = A_1 \cos \alpha\xi + B_1 \cosh \alpha\xi + \frac{\lambda h_o c^2}{2EI\alpha^4} \tag{22}$$

Substitution of equation (22) into the boundary conditions for the symmetrical solution (eqs. (18) and (19)) yields, respectively,

$$A_1 = \frac{\cosh \alpha}{\cos \alpha} B_1 \tag{23}$$

$$\frac{B_1}{\lambda} \cosh \alpha = \frac{-\frac{4h_o}{c}\left(1 - \frac{3kc^3}{4Et^3\alpha^4}\right)}{EI \frac{8\alpha^3}{c^3}(\tan \alpha + \tanh \alpha) - k} \tag{24}$$

Note that three unknowns appear in equations (23) and (24): A_1, B_1, and λ. However, by substituting equation (22) for w into equation (17) for λ and performing the necessary integration, a third expression is obtained:

$$\lambda = \frac{8h_o tE}{c^2} B_1 \cosh \alpha\left(-2 + \frac{\tan \alpha + \tanh \alpha}{\alpha}\right) \tag{25}$$

If $B_1 \frac{\cosh \alpha}{\lambda}$ in equation (25) is replaced by its identity in equation (24), the characteristic or frequency equation is found, and can be written as

$$1 = \frac{48\left(\frac{h_o}{t}\right)^2\left[2\alpha - (\tan \alpha + \tanh \alpha)\right]\left[1 - \frac{3k}{4E\alpha^4}\left(\frac{c}{t}\right)^3\right]}{\alpha^4(\tan \alpha + \tanh \alpha) - \frac{3k\alpha}{2E}\left(\frac{c}{t}\right)^3} \tag{26}$$

10

Substitution of equations (23) and (25) into equation (22) yields the mode shape

$$w = \frac{\cos \alpha\xi}{\cos \alpha} + \frac{\cosh \alpha\xi}{\cosh \alpha} - \left[\frac{\dfrac{\tan \alpha + \tanh \alpha}{\alpha} - \dfrac{3k}{2E\alpha^4}\left(\dfrac{c}{t}\right)^3}{1 - \dfrac{3k}{4E\alpha^4}\left(\dfrac{c}{t}\right)^3}\right] \tag{27}$$

Antisymmetrical solution.- In the antisymmetrical solution the mid-plane force λ is zero, as can be seen from equation (6). In equation (6) the integrand of the integral expression for λ is an antisymmetrical function about $c/2$; consequently its integral from 0 to c is zero. The differential equation for the cross section, given by equation (15), and the boundary conditions given by equations (10) and (11) therefore reduce to

$$\frac{d^4w}{d\xi^4} - \alpha^4 w = 0 \tag{28}$$

and

$$\left.\frac{d^2w}{d\xi^2}\right|_{\xi=1} = 0 \tag{29}$$

$$\left.\left(\frac{2}{c}\right)^3 EI \frac{d^3w}{d\xi^3} - \frac{k}{2} w\right|_{\xi=1} = 0 \tag{30}$$

Equations (28) to (30) are the differential equation and boundary conditions for a beam supported by springs at $\xi = -1$ and $\xi = 1$. The solution is presented in most vibration text books, but for the sake of completeness it will be repeated here. For the antisymmetrical solution

$$w = A_2 \sin \alpha\xi + B_2 \sinh \alpha\xi \tag{31}$$

Substitution of equation (31) into the boundary conditions yields

$$A_2 = \frac{\sinh \alpha}{\sin \alpha} B_2 \tag{32}$$

$$\alpha^3\left(\frac{2}{c}\right)^3 EI\left(-A_2 \cos \alpha + B_2 \cosh \alpha\right) = \frac{k}{2}\left(A_2 \sin \alpha + B_2 \sinh \alpha\right) \tag{33}$$

L
1
4
4
4

Thus, the characteristic or frequency equation becomes

$$\frac{\coth \alpha - \cot \alpha}{2\alpha} = \frac{3k}{4E\alpha^4}\left(\frac{c}{t}\right)^3 \tag{34}$$

and the mode shape is

$$w = \frac{\sin \alpha\xi}{\sin \alpha} + \frac{\sinh \alpha\xi}{\sinh \alpha} \tag{35}$$

NUMERICAL RESULTS FOR IDEALIZATION OF MONOCOQUE WING

WITH SYMMETRICAL PARABOLIC CROSS SECTION

Symmetrical Modes

The exact frequency and mode-shape equations of the idealized structure were obtained in the previous section. In equation (26) the frequency parameter α $\left(\text{where } \omega = \alpha^2\sqrt{\frac{16EI}{c^4\rho t}}\right)$ of the symmetrical modes was given as a function of t/h_0 and the parameter $\frac{k}{E}\left(\frac{c}{t}\right)^3$. The motion of the idealized structure can be considered to be the result of the coupling of two types of modes of vibration: an infinite set of uncoupled cross-sectional modes which are obtained by omitting the springs, and a rigid-body mode represented by a rigid cross section mounted on springs. Consequently, if the vibrations are considered in this light a more useful parameter than $\frac{k}{E}\left(\frac{c}{t}\right)^3$ would be $\omega_{r,B}/\omega$, where $\omega_{r,B}$ is the rigid-body translation frequency and is defined by $\omega_{r,B} = \sqrt{\frac{k}{\rho tc}}$, so that

$$\left(\frac{\omega_{r,B}}{\omega}\right)^2 = \frac{3k}{4E\alpha^4}\left(\frac{c}{t}\right)^3 \tag{36}$$

Thus the frequency equation (26) becomes

$$\frac{\left[\left(\frac{t}{h_o}\right)^2 \frac{\alpha^4}{48} - 1\right]\dfrac{2\alpha}{\tan \alpha + \tanh \alpha} + 1}{\left[\left(\frac{t}{h_o}\right)^2 \frac{\alpha^4}{48} + 1\right] - \dfrac{2\alpha}{\tan \alpha + \tanh \alpha}} = \left(\frac{\omega}{\omega_{r,B}}\right)^2 \tag{37}$$

and the corresponding mode shape (eq. (27)) is given by

$$w = \frac{\cos \alpha \xi}{\cos \alpha} + \frac{\cosh \alpha \xi}{\cosh \alpha} - \frac{\dfrac{\tan \alpha + \tanh \alpha}{\alpha} - 2\left(\dfrac{\omega_{r,B}}{\omega}\right)^2}{1 - \left(\dfrac{\omega_{r,B}}{\omega}\right)^2} \qquad (38)$$

The coupled frequency coefficient α was calculated from equation (37) for various values of $\left(\dfrac{t}{h_0}\right)^2$ and $\left(\dfrac{\omega_{r,B}}{\omega}\right)^2$ and the results are shown in figure 3. Here the frequency coefficient α for the first three modes is plotted as a function of $\left(\dfrac{\omega}{\omega_{r,B}}\right)^2$ for a range of $\left(\dfrac{t}{h_0}\right)^2$ from 0 to 0.09. As $\left(\dfrac{\omega}{\omega_{r,B}}\right)^2$ becomes greater than 1, all curves approach horizontal asymptotes whose values depend on $\dfrac{t}{h_0}$. These asymptotes have the value of the uncoupled cross-sectional frequencies obtained by letting $k = 0$ which correspond to the case where no coupling exists between rigid and cross-sectional motion. Consequently the mode shapes associated with these frequencies are ones which are predominantly cross sectional in character - that is, they contain two or more nodal points.

For k equal to zero, equation (37) reduces to the frequency equation for the uncoupled cross-sectional mode:

$$\left(\frac{t}{h_0}\right)^2 = \frac{48}{\alpha_c{}^4}\left(\frac{2\alpha_c}{\tan \alpha_c + \tanh \alpha_c} - 1\right) \qquad (39)$$

and equation (38) reduces to the corresponding uncoupled cross-sectional mode shape:

$$w = \frac{\cos \alpha_c \xi}{\cos \alpha_c} + \frac{\cosh \alpha_c \xi}{\cosh \alpha_c} - \frac{2}{\dfrac{\alpha_c{}^4}{48}\left(\dfrac{t}{h_0}\right)^2 + 1} \qquad (40)$$

where

$$\alpha_c = \sqrt[4]{\sqrt{\frac{c^4 \rho t \omega_c{}^2}{16EI}}} \qquad (41)$$

In figures 4(a) and 4(b), α_c is shown plotted as a function of $\left(\dfrac{t}{h_o}\right)^2$ for the first two symmetrical frequencies. These plots serve to determine the uncoupled chordwise frequency which corresponds to the pure chordwise modes of an infinitely long wing.

Values at $\left(\dfrac{\omega}{\omega_{r,B}}\right)^2 = 0$ in figure 3 describe the condition where the ends of the cross section are pinned; that is, $k = \infty$. Hence, mode shapes for $\dfrac{\omega}{\omega_{r,B}} \ll 1$ are also of predominantly chordwise character.

For values of $\dfrac{\omega}{\omega_{r,B}}$ approximately equal to 1 the curves approach a vertical asymptote $\left(\dfrac{\omega}{\omega_{r,B}}\right) = 1$ and correspond to the condition where the mode shapes are of the rigid-body type; that is, they contain no nodal points. As can be seen from figure 3, when $\left(\dfrac{t}{h_o}\right) = 0$ the curves fall on the asymptotes and no coupling exists. This uncoupling of the two motions could also have been surmised by examining the mode shape as given by equation (38). Note that for $\left(\dfrac{t}{h_o}\right)^2 = 0$ the tip deflections of the cross section in equation (38) are zero, and hence the stiffness of the springs can have no influence on the overall motion. The differences between the curves and their corresponding asymptotes for the other values of $\left(\dfrac{t}{h_o}\right)^2$ represent the change in frequency due to coupling between the chordwise and rigid motions. As can be seen from the plots, the greatest effect is felt when $\omega < \omega_{r,B}$.

One drawback with the curves presented in figure 3 is the difficulty encountered in using these curves to calculate the coupled frequency, since the unknown coupled frequency coefficient α appears in both the abscissa and ordinate of the curves. Thus the results of figure 3 have been replotted in figures 5(a) and 5(b) in terms of slightly different parameters.

In figures 5(a) and 5(b) the ratio of the coupled frequency ω to the rigid-body frequency $\omega_{r,B}$ is plotted as a function of the ratio of the fundamental uncoupled chordwise frequency $\omega_{c,1}$ to the rigid-body frequency $\omega_{r,B}$. Figure 5(a) presents the data for values of $\dfrac{\omega_{c,1}}{\omega_{r,B}}$

from 0 to 4.8 and $\frac{\omega}{\omega_{r,B}}$ from 0 to 3.2. Figure 5(b) is simply an enlargement of figure 5(a) in the region where $\frac{\omega_{c,1}}{\omega_{r,B}}$ goes from 0 to 2.0. The values of $\omega_{c,1}$ in the abscissa are based on the first uncoupled symmetrical mode for $k = 0$. Hence the abscissa depends only on the stiffness properties of the structure and not on the frequency parameter. The vertical asymptote of figure 3 appears in figure 5 as a horizontal line at $\frac{\omega}{\omega_{r,B}} = 1.0$, while the horizontal asymptotes of figure 3 transform into straight lines which emanate from the origin. Note that only the $\left(\frac{t}{h_o}\right)^2 = 0$ asymptotes appear in figure 5, since the asymptotes for all other values of $\left(\frac{t}{h_o}\right)^2$ lie in such close proximity to the $\left(\frac{t}{h_o}\right)^2 = 0$ asymptotes that they cannot be easily distinguished.

Figure 5 shows that for values of $\omega_{c,1}$ greater than $\omega_{r,B}$ the influence of coupling is appreciable only for the first or lowest mode, while for $\frac{\omega_{c,1}}{\omega_{r,B}} < 1$ all modes investigated show substantial effects. The frequencies of the coupled modes are easily obtained from figure 5, since the abscissa depends only on the physical properties which, of course, are assumed to be known. The difficulty lies in establishing the characteristics of the mode shapes - that is, in determining whether the resulting mode is predominantly a rigid mode with no nodal points or predominantly a chordwise mode with two or more nodal points.

In order to try to resolve this problem, the first three modes for $\left(\frac{t}{h_o}\right)^2 = 0.018$ and $\frac{\omega_{c,1}}{\omega_{r,B}} = 0.987$ and 0.409 were calculated and are shown in figures 6(a) and 6(b). From figure 6(a) it can be seen that the first mode is predominantly rigid-body motion while the remaining modes consist of chordwise-type motions. In figure 6(b), however, the second mode is the rigid-body-type mode. Presumably, as $\frac{\omega_{c,1}}{\omega_{r,B}}$ is reduced still further the third mode becomes the rigid-body mode and so on. In order to illustrate the change in mode shape due to coupling of chordwise and rigid-body motions, a sketch of the second mode for $\left(\frac{t}{h_o}\right)^2 = 0.018$ and various values of $\frac{\omega_{c,1}}{\omega_{r,B}}$ ranging from 0.026 to 0.987 is shown in figure 6(c).

From the foregoing discussion it can be seen that for $\dfrac{\omega_{c,1}}{\omega_{r,B}} > 1$ the

rigid mode is always the lowest mode. For $\dfrac{\omega_{c,1}}{\omega_{r,B}} < 1$ it is advisable to
calculate the mode shape in order to determine which mode is actually
the rigid-body mode.

In reference 4 the behavior of rectangular bents with flexible
members, mounted on either deflectional or rotational springs, has been
analyzed in detail.

It is of interest to note that the assumption of $h_O = 0$ $\left(\dfrac{t}{h_O} = \infty\right)$
in the present paper corresponds to the limiting case in reference 4
where the depth of the web is assumed to become zero while the thickness
becomes infinite. For such a configuration the frequency equations of
the two papers are found to be identical. This is true for both the
symmetrical and the antisymmetrical modes.

Antisymmetrical Modes

For the antisymmetrical modes, the frequency parameter α as given
in equation (34) is a function of $\dfrac{k}{E}\left(\dfrac{c}{t}\right)^3$ only. This lack of dependence
of frequency on camber in the antisymmetrical modes is a consequence of
the vanishing of the midplane force λ. Therefore, the equations for
the mode shapes and frequencies are those of the antisymmetrical vibra-
tions of a beam mounted on spring supports. As was true for the symmet-
rical modes, the motion of the idealized structure can be considered as
a result of the coupling between cross-sectional modes and rigid-body
modes. In the antisymmetrical case, however, the rigid-body mode is a

pitching or torsional mode. Hence, a more useful parameter than $\dfrac{k}{E}\left(\dfrac{c}{t}\right)^3$

is $\left(\dfrac{\omega_{r,T}}{\omega}\right)^2$, in which $\omega_{r,T}$ is now defined by

$$\omega_{r,T}^2 = \frac{3k}{\rho t c} \qquad (42)$$

The parameter $\omega_{r,T}$ can be looked upon as a rigid-body torsion mode
represented by the well-known equation

$$\omega_{r,T}^2 = \frac{K}{I_p} \qquad (43)$$

where

$$K = 2k\left(\frac{c}{2}\right)^2 \qquad (44)$$

and

$$I_p = \frac{\rho t c^3}{6} \qquad (45)$$

Note that I_p is the approximate polar moment of inertia for a thin cross section. The characteristic or frequency equation (eq. (34)) can then be written as

$$\frac{3}{2}\frac{\coth \alpha - \cot \alpha}{\alpha} = \left(\frac{\omega_{r,T}}{\omega}\right)^2 \qquad (46)$$

The mode shape is not an explicit function of the spring constant and remains

$$w = \frac{\sin \alpha \xi}{\sin \alpha} + \frac{\sinh \alpha \xi}{\sinh \alpha} \qquad (47)$$

The coupled frequency coefficient α was calculated from equation (46) for various values of $\left(\frac{\omega}{\omega_{r,T}}\right)^2$ and the results are shown in figure 7. In figure 7 the first three modes of α are plotted as a function of $\left(\frac{\omega}{\omega_{r,T}}\right)^2$. The uncoupled cross-sectional modes are represented by dashed horizontal lines, at $\alpha = 3.927$ and 7.069, for $k = 0$. The pin-ended condition for $k = \infty$ is represented by the dashed lines at $\alpha = \pi$, 2π, and 3π. The rigid-body torsion mode is the dashed vertical line at $\frac{\omega}{\omega_{r,T}} = 1$. The coupled modes are shown by the curved lines.

The corresponding plot of $\frac{\omega}{\omega_{r,T}}$ as a function of $\frac{\omega_{c,1}}{\omega_{r,T}}$ is shown in figure 8. The values of $\omega_{c,1}$ in the abscissa are based on the first uncoupled antisymmetrical mode for $k = 0$. The results are plotted in a manner similar to that for the symmetrical modes but only one curve is presented for each mode, the results being independent of the $\frac{t}{h_0}$ or camber effect. The dashed horizontal line at $\frac{\omega}{\omega_{r,T}} = 1.0$ represents

the rigid-body torsion mode, and the dashed straight lines inclined to the abscissa represent the uncoupled chordwise modes.

Contrary to the case of the symmetrical modes, the predominantly rigid-body mode with no nodal points is easily distinguished, as it is always the first or fundamental mode.

APPLICATION OF METHOD

The present paper has two objectives: (1) to analyze the chordwise vibrational characteristics of thin wings with airfoil-type cross sections and (2) to obtain the effect of the coupling between the chordwise and spanwise motions of the structure. Both of these objectives can be accomplished by utilizing the results obtained from the analyses of the simplified model.

In principle, the method presented is similar to that discussed in references 3 and 4. In the present investigation, however, emphasis is placed on the determination of the predominantly chordwise modes and frequencies of the structure in addition to the modes and frequencies of the overall beam motions. The results obtained from the analysis for the model with springs can be used to give both the chordwise and the spanwise coupled frequencies provided, of course, that the appropriate choice of the spring constant is made. The uncoupled cross-sectional modes and frequencies can be obtained from the analysis by letting the spring constant vanish.

Since the rigid-body motion of the idealized structure depends only on the spring constant while the relative chordwise motion depends on the flexibility of its members, the value of the spring constant should be chosen so that the uncoupled rigid-body frequency (either translational or torsional) of the idealized structure is the same as the spanwise frequency of the prototype. For the symmetrical chordwise modes the spring constant should be determined from the frequencies of the spanwise bending modes by means of the equation

$$k = \omega_{r,B}^2 \rho t c \tag{48}$$

while for the antisymmetrical chordwise modes the spring constant should be determined from the spanwise torsional frequencies by means of the equation

$$k = \omega_{r,T}^2 \frac{\rho t c}{3} \tag{49}$$

The spanwise frequency of the prototype should be obtained by the most appropriate method available, with the provision that the method be based on the assumption that the cross section of the structure remain undistorted.

At this time a note of caution as to the application of the method presented is in order. The use of the idealized structure embodies the assumption that all cross sections distort identically. Hence the influence of any bulkhead, rib, or other chordwise restraint is not included. Consequently, the method is applicable only to wings in which the bulkhead spacing is not very small.

In order to demonstrate the use of the method, both the coupled chordwise and coupled spanwise modes and frequencies of a circular-arc monocoque beam used in the experimental investigation of reference 2 will be calculated. For the sake of completeness a short description of the specimen used and the results obtained will be presented in this paper.

The aluminum monocoque beam was 140 inches long and 40 inches wide. The nominal dimensions and average radius of curvature are shown in figure 9. The beam had a ratio $\dfrac{h_o}{c}$ of approximately 0.04 and a ratio $\left(\dfrac{t}{h_o}\right)^2$ of 0.06735. The cross sections were maintained by steel bulkheads located 10 inches from each spanwise tip. Eighteen bending and torsional modes were found, and in addition a number of so-called "panel" modes were located. (See figs. 5 and 7 of ref. 2.)

From a comparison of the spanwise node lines shown in reference 2 and the mode shapes shown in figure 6, it can be concluded that many of these panel modes can be described as chordwise modes. The variation in position of the chordwise node lines is the result of coupling of the symmetrical chordwise modes with the beam bending modes or coupling of the antisymmetrical chordwise modes with the beam torsional modes. Consequently, a family of chordwise modes is associated with each of the spanwise modes. An additional node line appears at each spanwise end of some of the chordwise modes. These node lines result from the rigid tip bulkheads used in the construction of the specimens.

Since the covers of the monocoque beam were uniform in thickness and the camber of the cross section can be closely approximated by a parabola, the exact solution previously discussed is applicable. Hence the predominantly chordwise and predominantly spanwise frequencies of the monocoque including the influence of coupling can be obtained directly from figures 5 and 8.

Before this can be done, however, the uncoupled beam frequencies $\omega_{r,B}$ and $\omega_{r,T}$ and the uncoupled cross-sectional frequency $\omega_{c,1}$ must be obtained. The uncoupled chordwise frequency $\omega_{c,1}$ was calculated with the use of the curves in figure 4(a) or equation (39) for symmetrical frequencies and equation (34) (with k = 0) for the antisymmetrical case. The uncoupled chordwise frequencies are listed at the top of tables I and II. The bending frequencies of the beam were calculated in reference 2 by methods which include effects of transverse shear and shear lag, and the torsional beam frequencies by methods which include restraint of warping. These beam frequencies are listed in column ② of tables I and II.

In the first column of tables I and II is shown a sketch of the nodal pattern under consideration. The modes are grouped in pairs, except for the first, with each pair consisting of a spanwise mode and the corresponding first coupled chordwise mode. (The higher chordwise modes were not obtained experimentally and thus are not included.) The first mode in column ① of each table is the chordwise mode associated with each of the rigid-body spanwise modes. The ratios $\dfrac{\omega_{c,1}}{\omega_{r,B}}$ and $\dfrac{\omega_{c,1}}{\omega_{r,T}}$ are shown in column ③ of tables I and II, respectively. The corresponding frequency ratios $\dfrac{\omega}{\omega_{r,B}}$ and $\dfrac{\omega}{\omega_{r,T}}$ were obtained from figures 5 and 8 and are tabulated in column ④. For the predominantly beam modes this ratio represents the reduction in beam frequency due to cross-sectional deformations. In an attempt to evaluate the results, the calculated coupled frequency ω is presented in column ⑤ and the experimental frequency in column ⑥.

In table I (for bending) the predominantly beam modes show little effect due to coupling at the low frequencies. At the higher modes, however, the coupling effect becomes appreciable, and it is encouraging to note the good agreement between calculated and experimental frequencies. This good agreement at the higher modes can also be looked upon as an indication that the method is applicable to low-aspect-ratio wings.

In table II (for torsion) the predominantly beam modes are greatly affected by the coupling due to cross-sectional deformations, even at the low frequencies. However, the accuracy of prediction of the coupled frequencies at the higher modes indicates that the applicability of the method in torsion to low-aspect-ratio wings has limitations.

The calculated coupled chordwise frequencies show fair agreement with experimental frequencies and indicate that a large number of chordwise modes are present over a narrow frequency band, sometimes falling within a few cycles of each other. Unfortunately, as the investigation

presented in reference 2 was primarily concerned with beam modes, the experimental frequencies of the chordwise modes were not always obtained and some are missing in tables I and II. Further, because of the complexity of the nodal patterns, it was difficult in some instances to correlate the experimental and theoretical mode shapes. Though the correlation between the calculated and experimental chordwise frequencies is good, the application to low-aspect-ratio wings is open to question, as the accuracy of prediction is not well established at the higher frequencies.

It is to be noted that a second, thicker skinned monocoque beam was discussed in reference 2, but for a number of reasons it has not been presented or discussed here. First, the $\left(\dfrac{t}{h_o}\right)^2$ ratio of 0.356 for the thicker monocoque is felt to be straining the limits of some of the basic assumptions of the present analysis. Second, because of a much higher uncoupled chordwise frequency, the coupling effects on the beam frequencies in bending would be much smaller than in the lighter monocoque. Furthermore, the chord length and radius of curvature used in the calculations of the uncoupled beam frequencies $\omega_{r,B}$ and $\omega_{r,T}$ are questionable, as the frequencies of the rigid-body beam modes $\omega_{r,B}$ calculated from these dimensions are lower than those observed experimentally. Since the theories used in these calculations do not include all the flexibilities of the actual structure, the calculated values should be higher than the experimental values, rather than lower. It may also be noted that the dimensions of maximum depth, chord length, and radius of curvature for the thicker beam are not compatible with those for a circular arc. When the radius of curvature was altered by 6 percent in order to describe a circular arc, a 12-percent change was noted in the third and fifth rigid-body modes. More than likely, then, the calculated rigid-body frequencies of the thicker beam are somewhat higher in magnitude than those calculated in reference 2.

CONCLUDING REMARKS

The vibrational behavior of thin wings with airfoil-type cross sections has been investigated by means of an analysis of an idealized structure consisting of two curved beams mounted on springs. The results obtained from an analysis of this model can be used not only to obtain the chordwise modes and frequencies of the prototype but also to obtain an estimate of the reduction in spanwise frequency due to the coupling effect between cross-sectional and spanwise motions. Both uncoupled chordwise frequencies and the resulting coupled chordwise and spanwise frequencies are presented for beams with uniform cover thickness and parabolic cross sections. A comparison is made with existing experimental

data on a circular-arc monocoque. The comparison shows good agreement for the coupled beam frequencies and fair agreement for the coupled chordwise frequencies at moderate aspect ratios. For beams of arbitrary cross section an approximate matrix procedure is also presented.

Langley Research Center,
 National Aeronautics and Space Administration,
  Langley Air Force Base, Va., September 21, 1961.

L
1
4
4
4

APPENDIX

APPROXIMATE SOLUTION OF AN ARBITRARY AIRFOIL SECTION

In this appendix an approximate solution for an idealized structure of arbitrary shape and variable thickness is presented. The energies of the system are expressed in discrete form by writing all derivatives as differences and all integrals as summations according to the trapezoidal rule. The deflections at discrete points are considered as the unknowns of the system. After the boundary conditions are properly accounted for, a system of linear simultaneous equations in terms of these unknowns is obtained by minimizing the energy function $U - T$.

From equations (4), (6), and (7) the expression for $U - T$ can be written as

$$U - T = \frac{1}{2} \int_0^c EI(w'')^2 dx + \frac{1}{c} \int_0^c Eth'w' dx \int_0^c h'w' dx + \frac{1}{4} k_1 w(c)^2$$

$$+ \frac{1}{4} k_2 w(0)^2 - \frac{\omega^2}{2} \int_0^c \rho t w^2 dx \tag{A1}$$

The first step in the procedure is to choose equally spaced stations along the x-axis, numbering them from $n = 0$ to $n = N$. Integrals can then be approximated, either in terms of values of the integrand at the full stations

$$\int_0^c f(x)dx = \Delta\left(\frac{f_0}{2} + f_1 + \ldots + f_{N-1} + \frac{f_N}{2}\right) \tag{A2}$$

or in terms of the values at the half stations

$$\int_0^c f(x)dx = \Delta\left[f_{1/2} + f_{3/2} + \ldots + f_{N-(1/2)}\right] \tag{A3}$$

where Δ is the equal distance between stations.

The first integral in equation (A1) is approximated by means of equation (A2), as the values of the second derivative appearing in the integrand are best approximated by differences at the full stations:

$$w'' \Big|_n \approx \frac{w_{n+1} - 2w_n + w_{n-1}}{\Delta^2} \tag{A4}$$

Consequently, the first integral can be written in matrix form as follows:

$$\frac{1}{2} \int_0^c EI(w'')^2 dx = \frac{1}{2\Delta^3} \lfloor w \rfloor \left[D_2^* \right]' \left[EI \right] \left[D_2^* \right] \lvert w \rvert \tag{A5}$$

where the definitions of the matrices are given below, and the number of rows and columns, in that order, are indicated beside each:

$$\lfloor w \rfloor = \lfloor w_{-1}, \ w_0, \ \cdots, \ w_{N+1} \rfloor \qquad (1) \times (N+3) \tag{A6}$$

$$\lvert w \rvert = \lfloor w \rfloor' \qquad (N+3) \times (1) \tag{A7}$$

$$\left[D_2^* \right] = \begin{bmatrix} 1 & -2 & 1 & & & & \\ & 1 & -2 & 1 & & & \\ & & & \cdots & & & \\ & & & & 1 & -2 & 1 \\ & & & & & 1 & -2 & 1 \end{bmatrix} \qquad (N+1) \times (N+3) \tag{A8}$$

$$\left[EI \right] = \begin{bmatrix} \left(\frac{EI}{2}\right)_0 & & & & \\ & (EI)_1 & & & \\ & & \cdots & & \\ & & & (EI)_{N-1} & \\ & & & & \left(\frac{EI}{2}\right)_N \end{bmatrix} \qquad (N+1) \times (N+1) \tag{A9}$$

A prime on a matrix denotes the transpose of the matrix.

Note that the values of w at stations corresponding to $n = -1$
and $n = N + 1$ (points not on the structure) appear in the matrices.
These points can be evaluated with the use of the finite-difference form
of the boundary conditions in equations (10) and (12):

$$EIw''\Big|_{n=N} = \frac{w_{n+1} - 2w_N + w_{N-1}}{\Delta^2} = 0 \qquad (A10)$$

and

$$EIw''\Big|_{n=0} = \frac{w_1 - 2w_0 + w_{-1}}{\Delta^2} = 0 \qquad (A11)$$

With the conditions expressed in equations (A10) and (A11), equa-
tion (A5) can be rewritten as

$$\frac{1}{2}\int_0^c EI(w'')^2 dx = \frac{1}{2\Delta^3}\lfloor w\rfloor \left[D_2\right]'\left[EI\right]\left[D_2\right]|w| \qquad (A12)$$

where now

$$\lfloor w\rfloor = \lfloor w_0, \ w_1, \ \ldots, \ w_N\rfloor \qquad (1)\times(N+1) \qquad (A13)$$

$$\left[D_2\right] = \begin{bmatrix} 1 & -2 & 1 & & & & \\ & 1 & -2 & 1 & & & \\ & & & \cdots & & & \\ & & & & 1 & -2 & 1 \\ & & & & & 1 & -2 & 1 \end{bmatrix} \qquad (N-1)\times(N+1) \qquad (A14)$$

$$\left[EI\right] = \begin{bmatrix} (EI)_1 & & \\ & \cdots & \\ & & (EI)_{N-1} \end{bmatrix} \qquad (N-1)\times(N-1) \qquad (A15)$$

The second integral in equation (A1) is approximated by the use of the values at the half stations (eq. (A3)), as the value of the first derivative appearing in the integrand is, in turn, best approximated by a half-station expression:

$$w'\Big|_{n+(1/2)} \approx \frac{w_{n+1} - w_n}{\Delta} \tag{A16}$$

Thus, by using both the half-station expressions (eqs. (A3) and (A16)) the second integral can be written in terms of the displacements at the full stations:

$$\frac{1}{c} \int_0^c Eth'w'dx \int_0^c h'w'dx = \frac{1}{c}\lfloor w \rfloor \left[D_1\right]'\left[h'\right]\left[Et\right]\left[h'\right]\left[D_1\right]\lfloor w \rfloor \tag{A17}$$

Here

$$\lfloor w \rfloor = \lfloor w_0, \; w_1, \; \cdots, \; w_N \rfloor \qquad (1)\times(N+1) \tag{A18}$$

$$\lfloor w \rfloor = \lfloor w \rfloor' \qquad (N+1)\times(1) \tag{A19}$$

$$\left[D_1\right] = \begin{bmatrix} -1 & 1 & & & & \\ & -1 & 1 & & & \\ & & & \cdots & & \\ & & & -1 & 1 & \\ & & & & -1 & 1 \\ & & & & & -1 \end{bmatrix} \qquad (N)\times(N+1) \tag{A20}$$

$$\left[h'\right] = \begin{bmatrix} h'_{1/2} & & & & \\ & h'_{3/2} & & & \\ & & \cdots & & \\ & & & h'_{N-(3/2)} & \\ & & & & h'_{N-(1/2)} \end{bmatrix} \qquad (N)\times(N) \tag{A21}$$

$$
\left[Et\right] = \begin{bmatrix} (Et)_{1/2} & (Et)_{1/2} & \cdot \cdot \cdot \\ (Et)_{3/2} & (Et)_{3/2} & \cdot \cdot \cdot \\ \cdot \cdot \cdot \cdot \cdot \cdot \cdot \cdot \cdot \cdot \cdot \cdot \cdot \\ (Et)_{N-(1/2)} & (Et)_{N-(1/2)} & \cdot \cdot \cdot \end{bmatrix} \quad (N) \times (N) \qquad (A22)
$$

The third term in equation (A1), or the potential energy of the spring mounts, is given in matrix form by

$$
\frac{1}{4} k_1 w(c)^2 + \frac{1}{4} k_2 w(0)^2 = \frac{1}{4} \lfloor w \rfloor \lceil k \rceil \lvert w \rvert \qquad (A23)
$$

where

$$
\left\lceil k \right\rceil = \begin{bmatrix} k_2 & & & & & \\ & 0 & & & & \\ & & 0 & & & \\ & & & \cdot \cdot \cdot & & \\ & & & & 0 & \\ & & & & & 0 \\ & & & & & & k_1 \end{bmatrix} \quad (N+1) \times (N+1) \qquad (A24)
$$

The last integral in equation (A1) is approximated by equation (A2):

$$
\frac{\omega^2}{2} \int_0^c \rho t w^2 dx = \frac{\omega^2}{2} \Delta \lfloor w \rfloor \lceil \rho t \rceil \lvert w \rvert \qquad (A25)
$$

where

$$
\left\lceil \rho t \right\rceil = \begin{bmatrix} \left(\frac{\rho t}{2}\right)_0 & & & & \\ & (\rho t)_1 & & & \\ & & \cdot \cdot \cdot & & \\ & & & (\rho t)_{N-1} & \\ & & & & \left(\frac{\rho t}{2}\right)_N \end{bmatrix} \quad (N+1) \times (N+1) \quad (A26)
$$

With equations (A12), (A17), (A23), and (A25) the energy function (eq. (A1)) can be written as

$$U - T = \lfloor w \rfloor \left[[A] - \frac{\omega^2}{2} [B] \right] | w |$$

(A27)

where

$$[A] = \frac{1}{2\Delta^3} [D_2]' [EI][D_2] + \frac{1}{c} [D_1]' [h'][Et][h'][D_1] + \frac{1}{4} [k]$$

(A28)

$$[B] = \Delta [\rho t]$$

(A29)

Application of the variation condition expressed in equation (8), $\delta(U - T) = 0$, where the variations are taken with respect to each w, results in

$$\left\{ \left[[A] + [A]' \right] - \frac{\omega^2}{2} \left[[B] + [B]' \right] \right\} | w | = 0$$

(A30)

Equation (A30) can be rewritten in a more usable form as

$$| w | = \frac{1}{\omega^2} [B]^{-1} \left[[A] + [A]' \right] | w |$$

(A31)

since

$$[B]' = [B]$$

(A32)

and the transpose of A is

$$[A]' = \frac{1}{2\Delta^3} [D_2]' [EI][D_2] + \frac{1}{c} [D_1]' [h'][Et]' [h'][D_1] + \frac{1}{4} [k]$$

(A33)

In order to establish the number of stations necessary to achieve reasonable accuracy with the finite-difference method, a brief comparison was made between the deflection shape of the first symmetrical mode as calculated from the exact solution presented for the monocoque wing of symmetrical parabolic cross section and the shape as calculated by finite-difference methods. Since a symmetrical mode was chosen for the comparison, only half of the doubly symmetrical parabolic-arc cross section was considered and the origin was moved to the midchord. (The limits of the integrals in eq. (A1) thus become 0 and $c/2$ instead of

0 and c.) With the additional simplification of constant cover thickness and constant material properties, equation (A31) reduces to

$$|w| = \frac{2}{c\eta\rho t\omega^2}[B]^{-1}2[A]|w| \tag{A34}$$

with

$$[B] = \begin{bmatrix} \frac{1}{2} & & & & & \\ & 1 & & & & \\ & & 1 & & & \\ & & & \cdots & & \\ & & & & 1 & \\ & & & & & 1 \\ & & & & & & \frac{1}{2} \end{bmatrix} \quad (N+1)\times(N+1) \tag{A35}$$

$$[A] = \frac{4EI}{c^3\eta^3}[D_3]'[K_1][D_3] + \frac{32h_o{}^2Et}{c^3}[D_1]'[K_2][K_3][K_2][D_1] + \frac{k}{4}[K_4]$$

$$(N+1)\times(N+1) \tag{A36}$$

$$\Delta = \frac{c}{2}\eta \tag{A37}$$

Since the origin is now located at the midchord the boundary condition originally given by equation (A11) (at $x = 0$) is replaced by that of symmetry at the midchord:

$$w_{-1} = w_1 \tag{A38}$$

and D_2 in equation (A33) becomes D_3 in equation (A36):

$$[D_3] = \begin{bmatrix} -2 & 2 & & & & & \\ 1 & -2 & 1 & & & & \\ & 1 & -2 & 1 & & & \\ & & & \cdots & & & \\ & & & 1 & -2 & 1 & \\ & & & & 1 & -2 & 1 \\ & & & & & 1 & -2 & 1 \end{bmatrix} \quad (N)\times(N+1) \tag{A39}$$

L
1
4
4
4

Furthermore,

$$
\begin{bmatrix} K_1 \end{bmatrix} = \begin{bmatrix} 1 & & & & \\ & 1 & & & \\ & & \cdots & & \\ & & & 1 & \\ & & & & 1 \end{bmatrix} \qquad (N)\times(N) \qquad\qquad (A40)
$$

$$
\begin{bmatrix} K_2 \end{bmatrix} = \begin{bmatrix} \frac{\eta}{2} & & & & \\ & \frac{3}{2}\eta & & & \\ & & \frac{5}{2}\eta & & \\ & & & \cdots & \\ & & & & \left(N-\frac{1}{2}\right)\eta \end{bmatrix} \qquad (N)\times(N) \qquad\qquad (A41)
$$

$$
\begin{bmatrix} K_3 \end{bmatrix} = \begin{bmatrix} 1 & 1 & \cdot & \cdot & \cdot \\ \cdot & \cdot & \cdot & \cdot & \cdot \\ \cdot & \cdot & \cdot & 1 & 1 \end{bmatrix} \qquad (N)\times(N) \qquad\qquad (A42)
$$

$$
\begin{bmatrix} D_1 \end{bmatrix} = \begin{bmatrix} -1 & 1 & & & & \\ & -1 & 1 & & & \\ & & \cdots & & & \\ & & & -1 & 1 & \\ & & & & -1 & 1 \\ & & & & & -1 & 1 \end{bmatrix} \qquad (N)\times(N+1) \qquad (A43)
$$

$$
\begin{bmatrix} K_4 \end{bmatrix} = \begin{bmatrix} 0 & & & & \\ & 0 & & & \\ & & \cdots & & \\ & & & 0 & \\ & & & & 0 \\ & & & & & 1 \end{bmatrix} \qquad (N+1)\times(N+1) \qquad (A44)
$$

L
1
4
4
4

If the rigid-body (translational) frequency is represented as

$$\omega_{r,B}^2 = \frac{k}{c\rho t}$$

with

$$I = \frac{t^3}{12}$$

$$\alpha^4 = \frac{c^4 \rho t \omega^2}{16 EI}$$

equation (A34) can be expressed in the parameters of the exact solution, and becomes

$$|w| = \frac{1}{\eta}[B]^{-1}\left\{ \frac{1}{\alpha^4 \eta^3}[D_3]'[K_1][D_3] \right.$$

$$\left. + \frac{96}{\alpha^4}\left(\frac{h_o}{t}\right)^2 [D_1][K_2][K_3][K_2][D_1] + \left(\frac{\omega_{r,B}}{\omega}\right)^2 [K_4] \right\}|w| \qquad (A45)$$

In figure 10 a plot of the first symmetrical mode shape of the parabolic-arc monocoque for $k = 0$ and $\left(\frac{t}{h_o}\right)^2 = 0.018$ is shown. The curve was calculated from equations (39) and (40) of the exact solution, and points were obtained from equation (A45) of the numerical procedure for 6, 9, and 11 stations across the half-chord. The error involved in predicting the overall frequencies, in comparison with the exact solution, is 6 percent for 6 stations, 2.5 percent for 9 stations, and less than 2 percent for 11 stations across the half-chord.
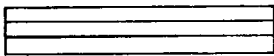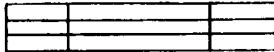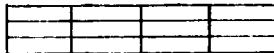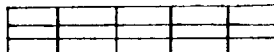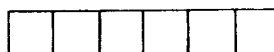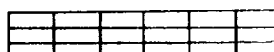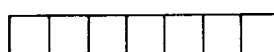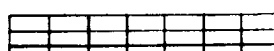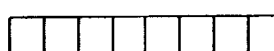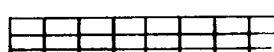
REFERENCES

1. Davidson, John R., Rosecrans, Richard, and Vosteen, Louis F.: Tests of Aerodynamically Heated Multiweb Wing Structures in a Free Jet at Mach Number 2 - Four Aluminum-Alloy Models of 20-Inch Chord and Span With 0.064-Inch-Thick Skin, 0.025-Inch-Thick Ribs and Webs, and Zero, One, Two, or Three Chordwise Ribs. NACA RM L57L13, 1958.

2. Fichter, Wilbur B., and Kordes, Eldon E.: Investigation of Vibration Characteristics of Circular-Arc Monocoque Beams. NASA TN D-59, 1959.

3. Kruszewski, Edwin T., and Davenport, William W.: Influence of Shear Deformation of the Cross Section on Torsional Frequencies of Box Beams. NACA TN 3464, 1955.

4. Budiansky, Bernard, and Fralich, Robert W.: Effects of Panel Flexibility on Natural Vibration Frequencies of Box Beams. NACA TN 3070, 1954.

5. Stein, Manuel, and Sanders, J. Lyell, Jr.: A Method for Deflection Analysis of Thin Low-Aspect-Ratio Wings. NACA TN 3640, 1956.

L
1
4
4
4

TABLE I.- NATURAL BENDING FREQUENCIES OF EXAMPLE BEAM[*]
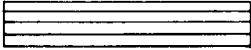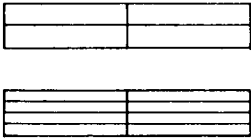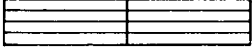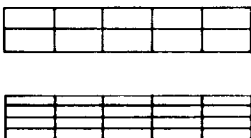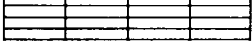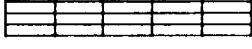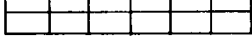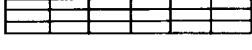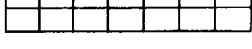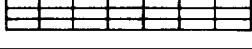
$$\left[\omega_{c,1} = \alpha_{c,1}^2 \sqrt{\frac{16EI}{c^4 \rho t}} = 107.85 \text{ cps}\right]$$

Mode ①	$\omega_{r,B}$, cps ②	$\dfrac{\omega_{c,1}}{\omega_{r,B}}$ ③	$\dfrac{\omega}{\omega_{?,B}}$ ④	ω, cps ⑤	ω_{exper}, cps ⑥
(single beam)				107.85	108.60
(beam)	17.01	6.340	0.993	16.89	16.95
(beam)			6.340	107.85	118.70
(beam)	40.95	2.634	0.964	39.50	40.05
(beam)			2.640	108	------
(beam)	71.24	1.514	0.895	63.75	63.36
(beam)			1.540	110	121.70
(beam)	105.40	1.023	0.800	84.00	83.75
(beam)			1.062	112	120.40
(beam)	145.70	0.740	0.660	96.20	102.30
(beam)			0.810	118	------
(beam)	188.20	0.573	0.537	101.00	114.70
(beam)			0.665	125	------

[*]Dimensions of beam are given in figure 9.

TABLE II.- NATURAL TORSIONAL FREQUENCIES OF EXAMPLE BEAM*

$$\left[\omega_{c,1} = \alpha_{c,1}^2 \sqrt{\frac{16EI}{c^4 \rho t}} = 82.13 \text{ cps}\right]$$

Mode (1)	$\omega_{r,T}$, cps (2)	$\dfrac{\omega_{c,1}}{\omega_{r,T}}$ (3)	$\dfrac{\omega}{\omega_{r,T}}$ (4)	ω, cps (5)	ω_{exper}, cps (6)
				82.13	------
	37.90	2.167	0.856	32.45	32.80
			2.510	95.30	------
	75.50	1.088	0.593	44.75	43.86
			1.670	126	109.20
	113.50	0.7236	0.434	49.30	50.52
			1.385	157	------
	152.10	0.540	0.347	52.80	57.73
			1.160	176	------
	192.60	0.4264	0.282	54.30	71.33
			0.970	187	------
	229.80	0.3575	0.240	55.20	89.10
			0.890	205	------

*Dimensions of beam are given in figure 9.
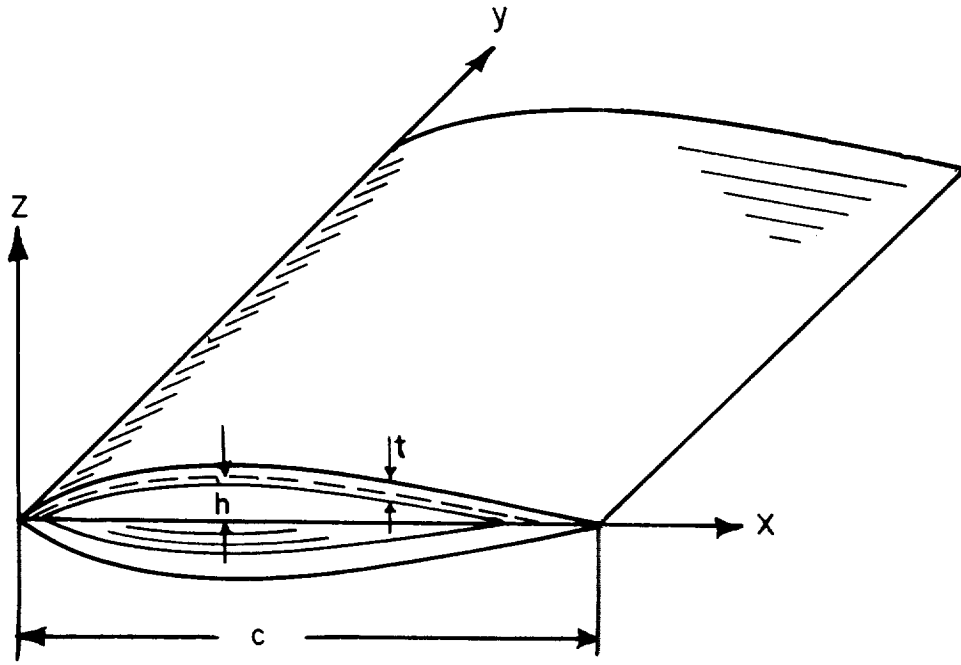
(a) Prototype.
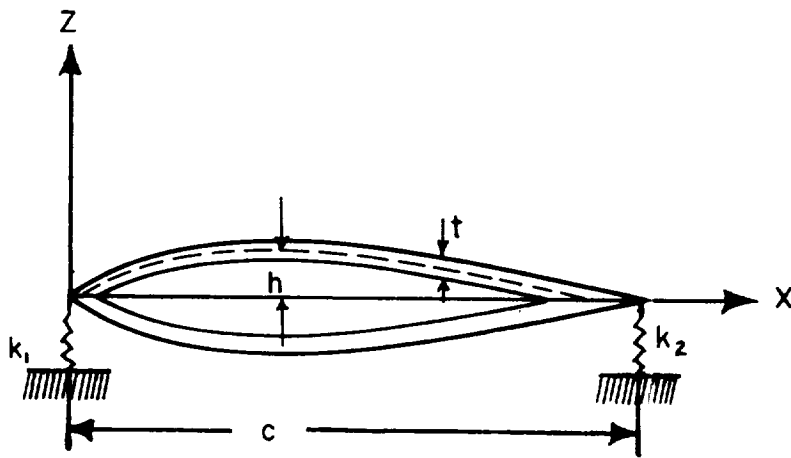
(b) Idealization.

Figure 1.- Thin airfoil-type cross section.
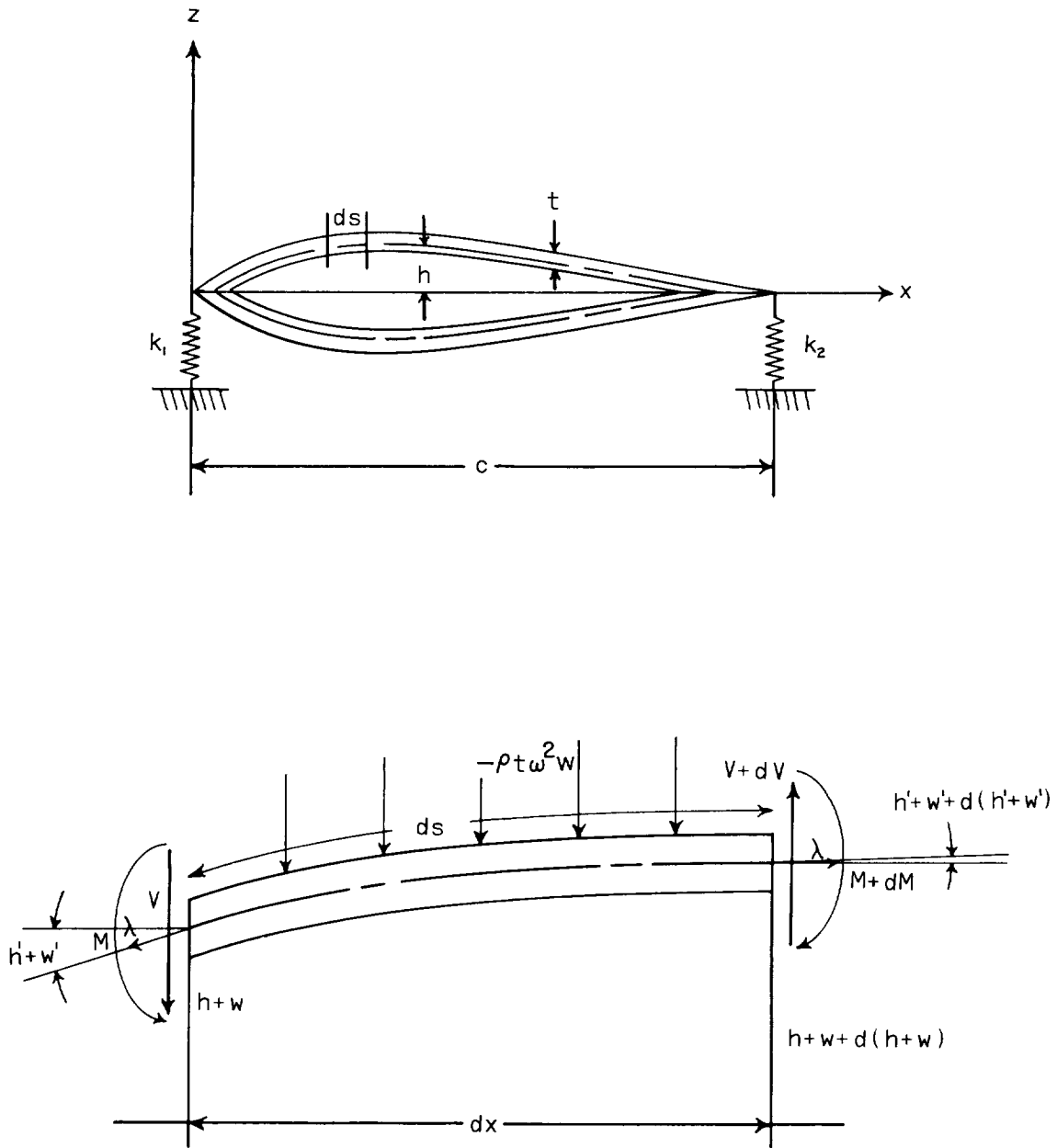
Figure 2.- Sign convention and coordinate system of idealized cross section.
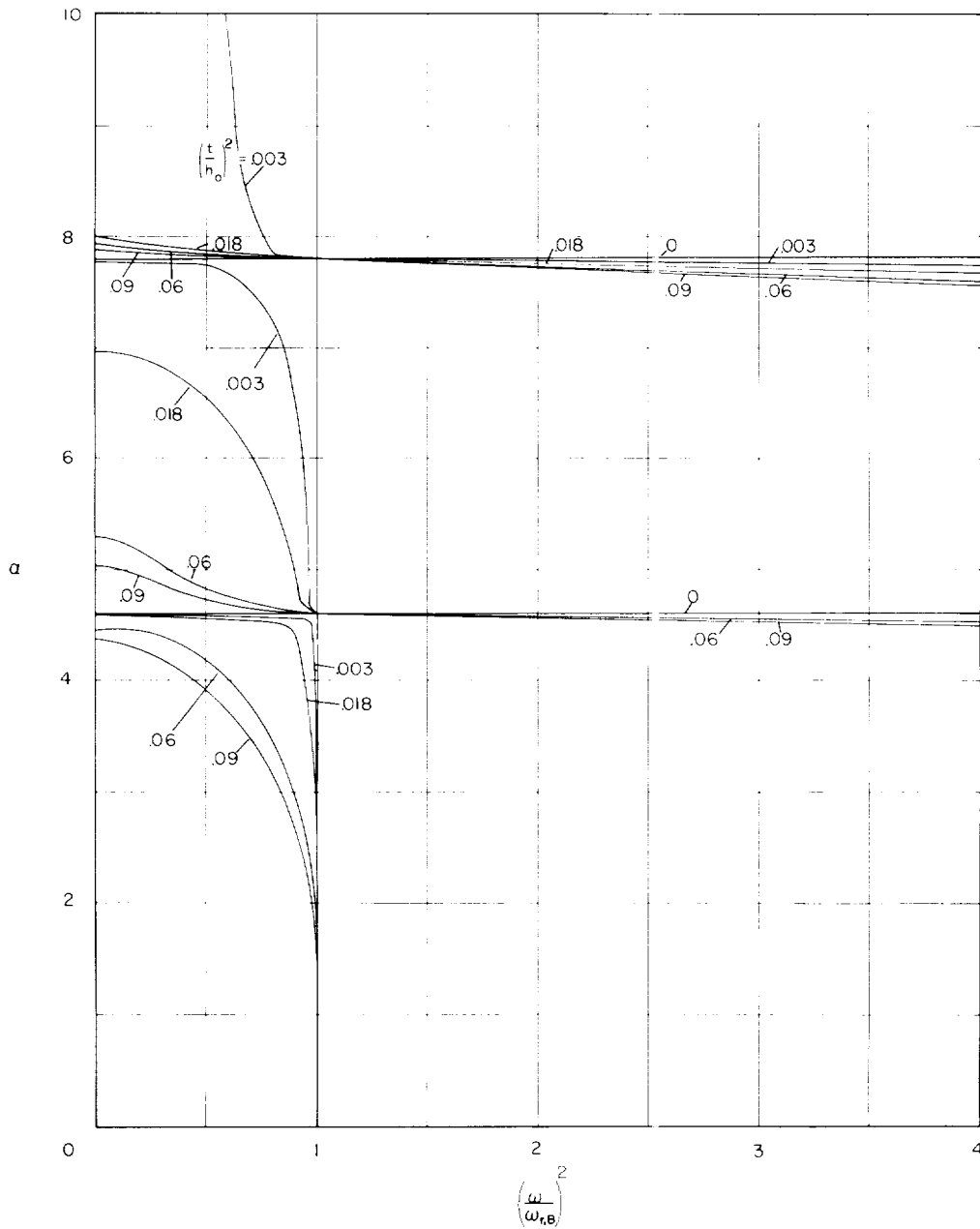
Figure 3.- Frequency coefficient as a function of frequency ratio

$$\left(\frac{\omega}{\omega_{r,B}}\right)^2 = \frac{\left[\left(\frac{t}{h_o}\right)^2 \frac{\alpha^4}{48} - 1\right]\dfrac{2\alpha}{\tan \alpha + \tanh \alpha} + 1}{\left[\left(\frac{t}{h_o}\right)^2 \frac{\alpha^4}{48} + 1\right] - \dfrac{2\alpha}{\tan \alpha + \tanh \alpha}}.$$
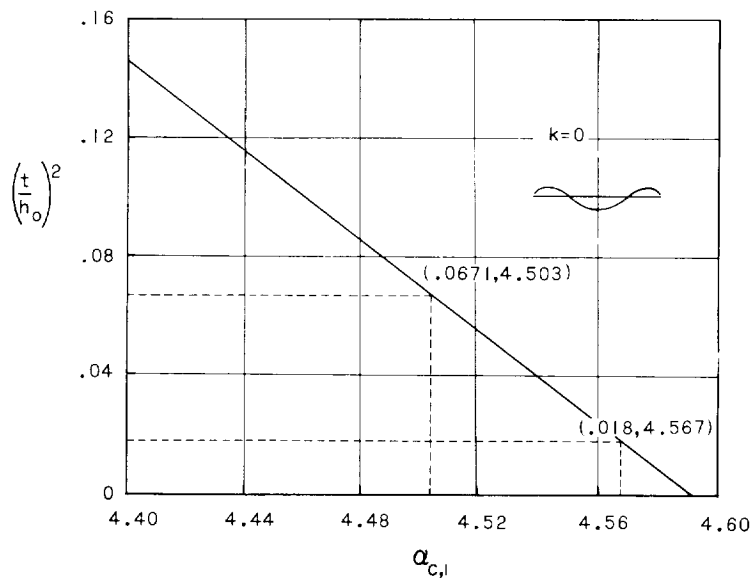
(a) First symmetrical frequencies.
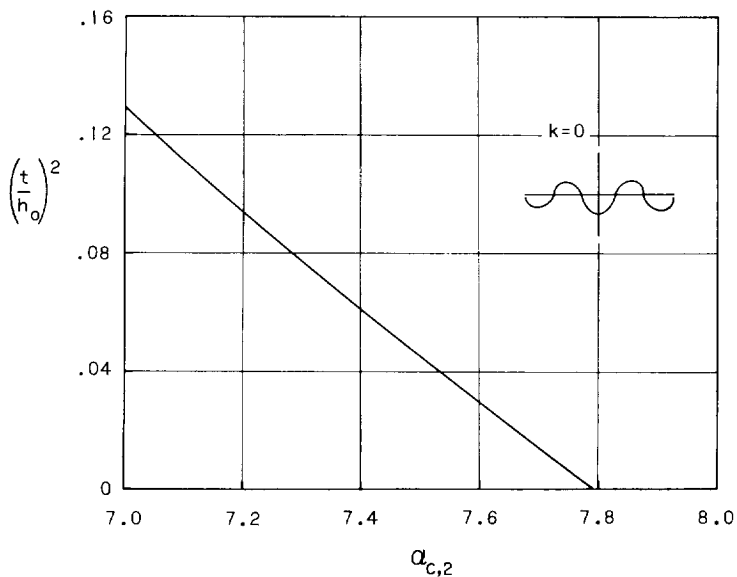
(b) Second symmetrical frequencies.

Figure 4.- Uncoupled chordwise frequency coefficient α_c as a function of $\left(\dfrac{t}{h_o}\right)^2 = \dfrac{48}{\alpha_c{}^4}\left(\dfrac{2\alpha_c}{\tan \alpha_c + \tanh \alpha_c} - 1\right)$.
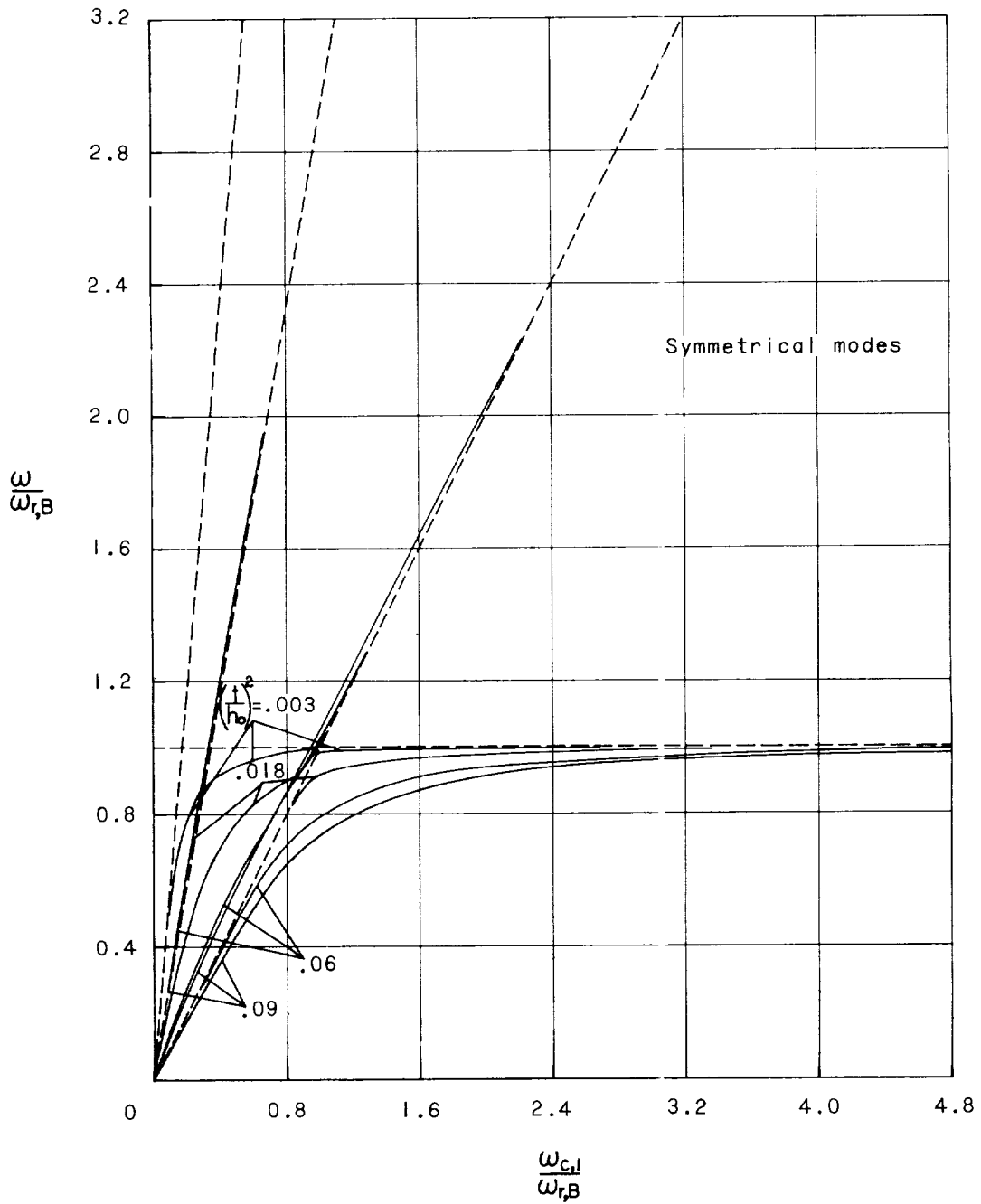
(a) $\dfrac{\omega_{c,1}}{\omega_{r,B}} = 0$ to 4.8.

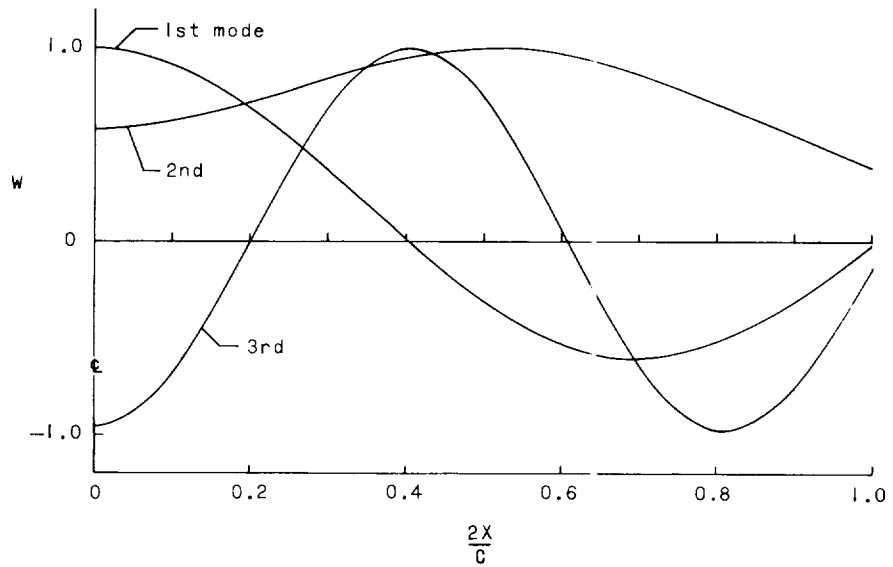Figure 5.- Variation of $\omega/\omega_{r,B}$ with $\omega_{c,1}/\omega_{r,B}$ for symmetrical modes.
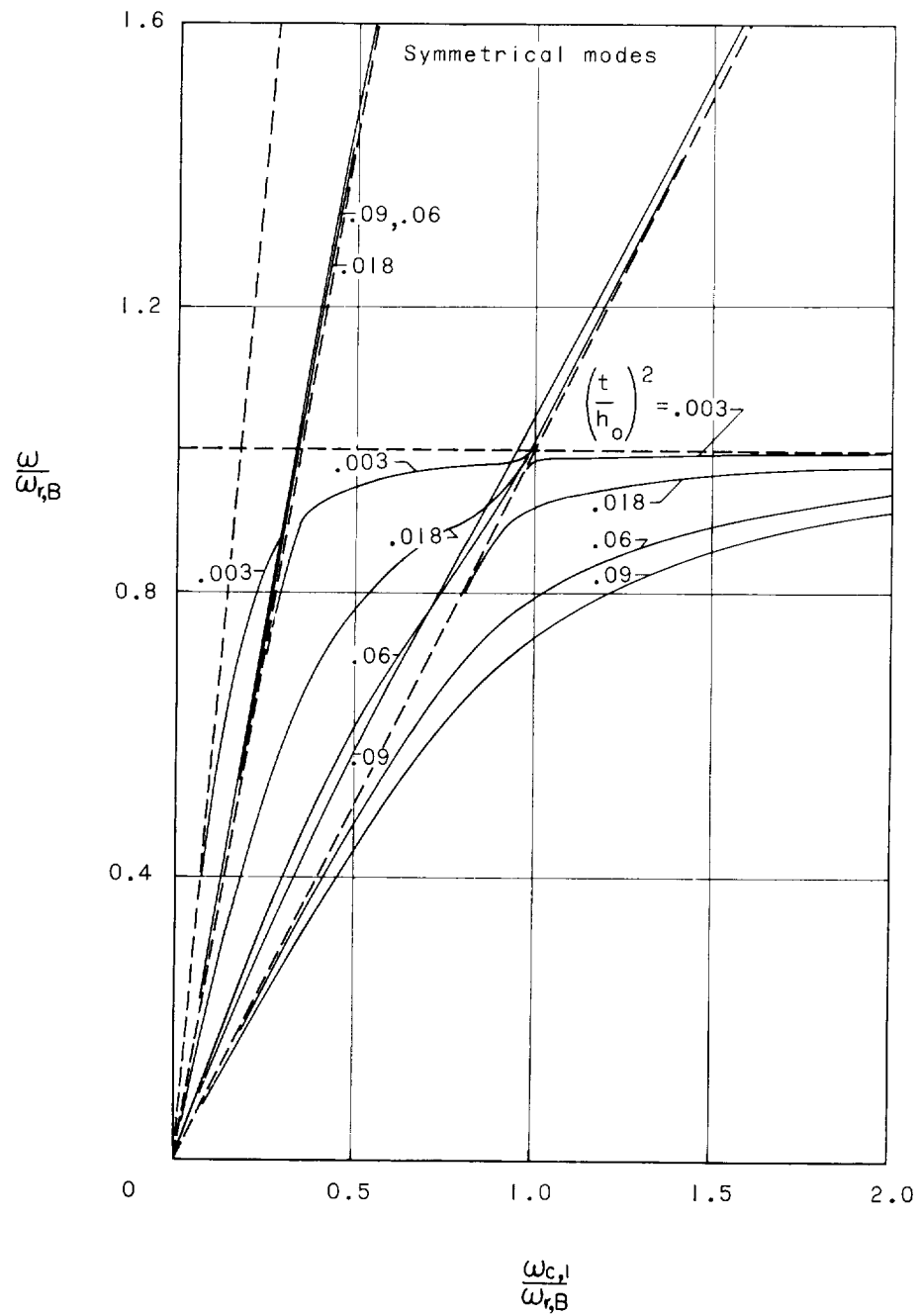
(b) $\dfrac{\omega_{c,1}}{\omega_{r,B}} = 0$ to 2.0.

Figure 5.- Concluded.
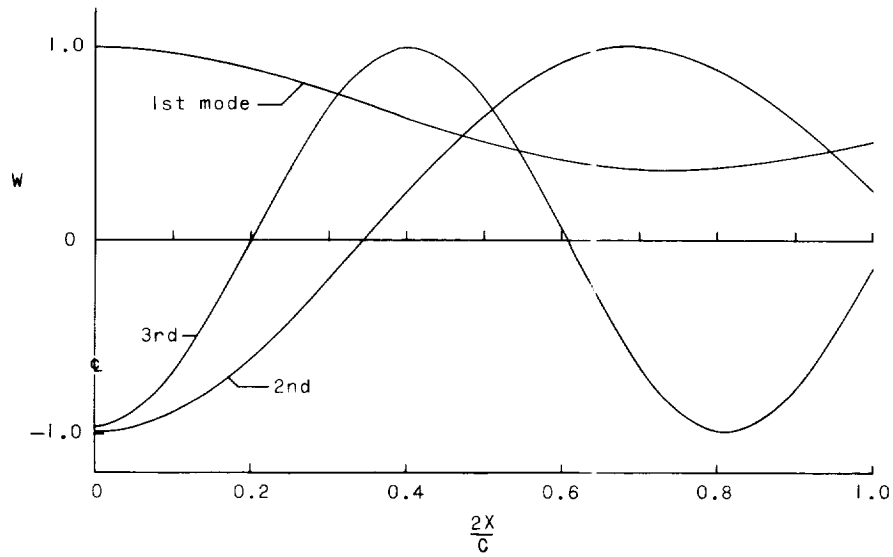
(a) $\dfrac{\omega_{c,1}}{\omega_{r,B}} = 0.987$.

(b) $\dfrac{\omega_{c,1}}{\omega_{r,B}} = 0.409$.

Figure 6.- Symmetrical mode shapes across the half-chord for $\left(\dfrac{t}{h_o}\right)^2 = 0.018$ and various values of $\dfrac{\omega_{c,1}}{\omega_{r,B}}$.

L-1444
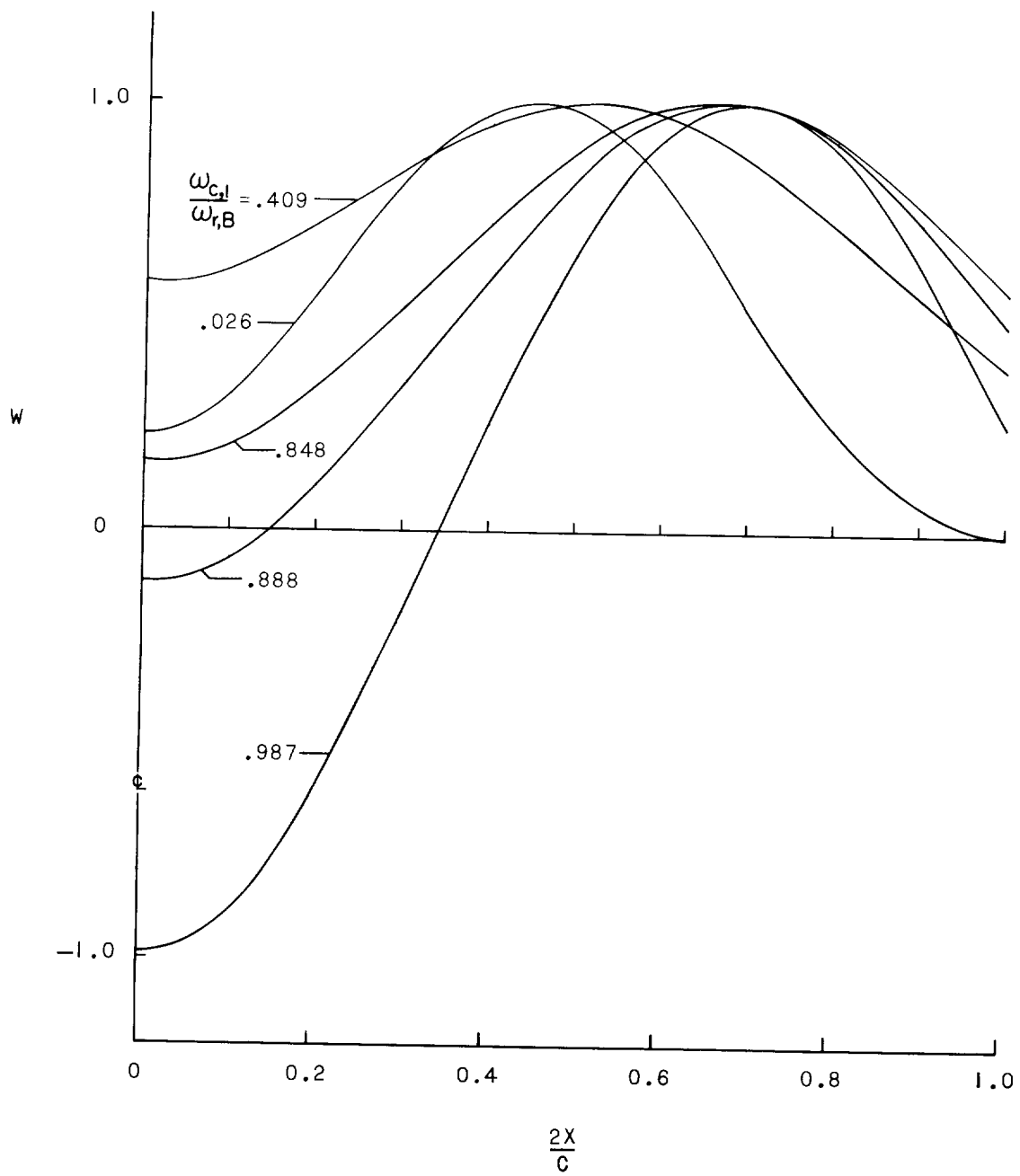
$$(c) \quad \frac{\omega_{c,1}}{\omega_{r,B}} = 0.987, \ 0.888, \ 0.848, \ 0.409, \ \text{and} \ 0.026.$$
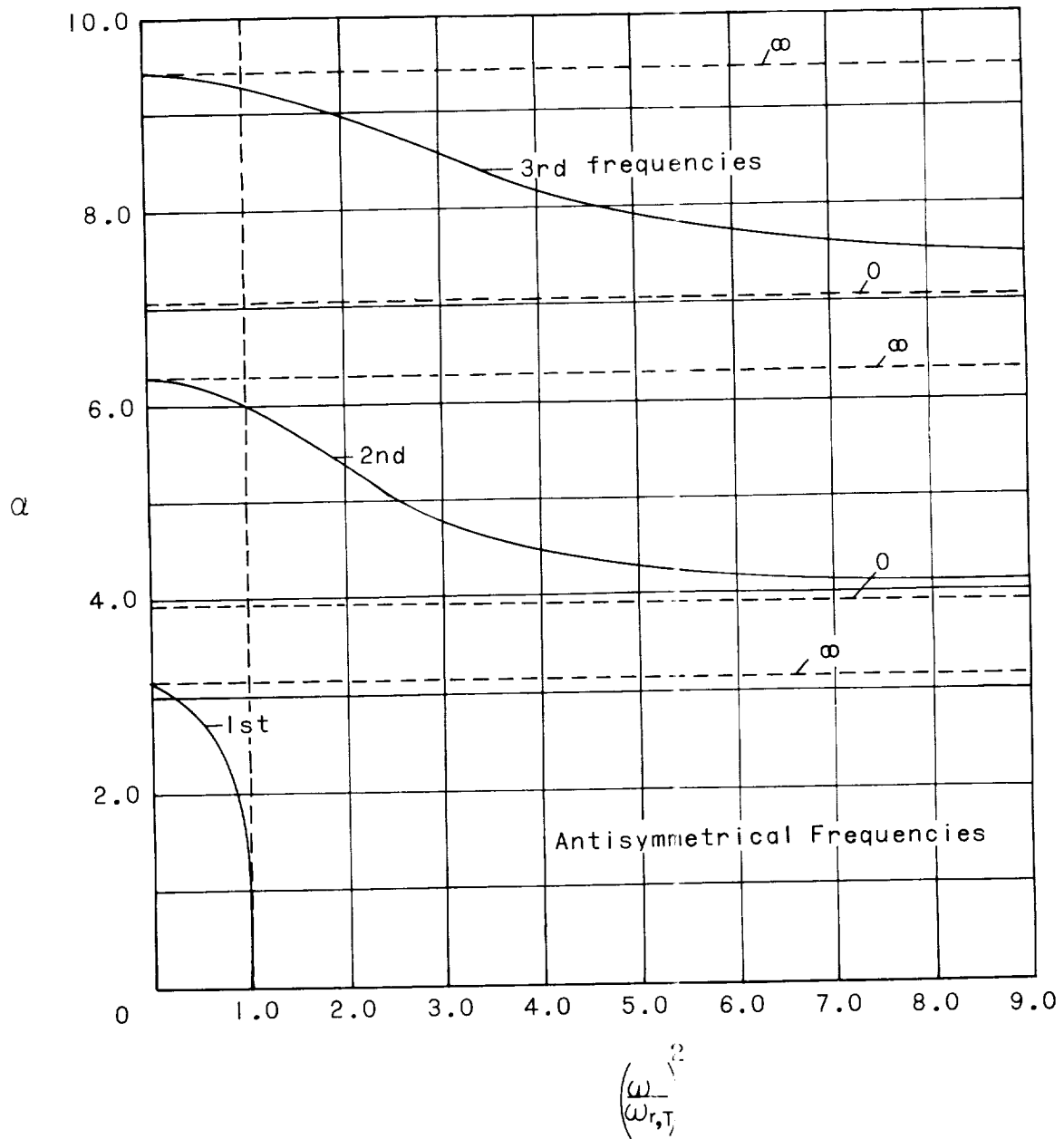
Figure 6.- Concluded.

Figure 7.- Frequency coefficient as a function of frequency ratio

$$\left(\frac{\omega}{\omega_{r,T}}\right)^2 = \frac{1}{\frac{3}{2\alpha}(\coth \alpha - \cot \alpha)}.$$
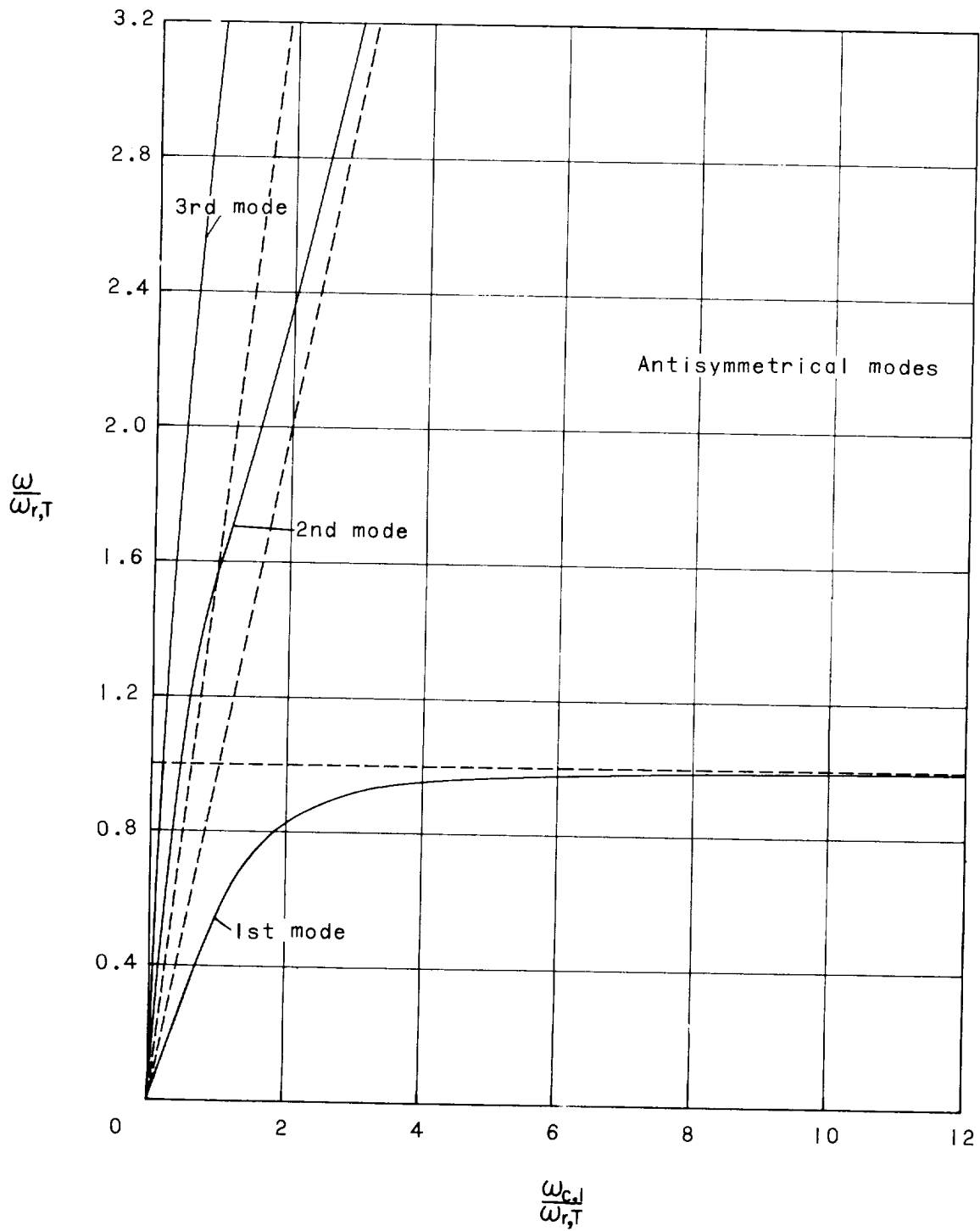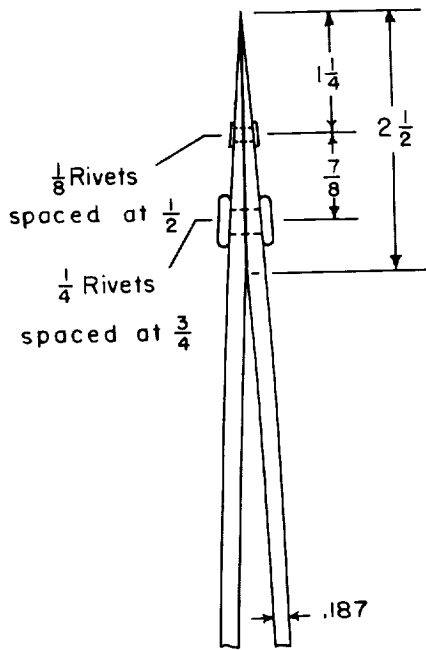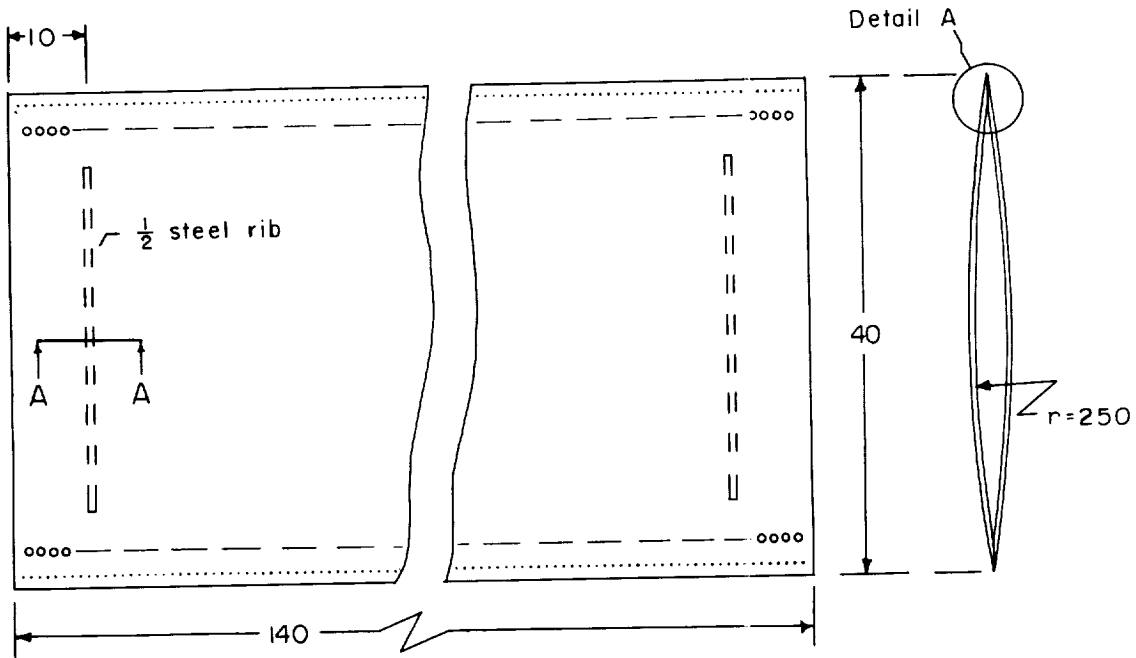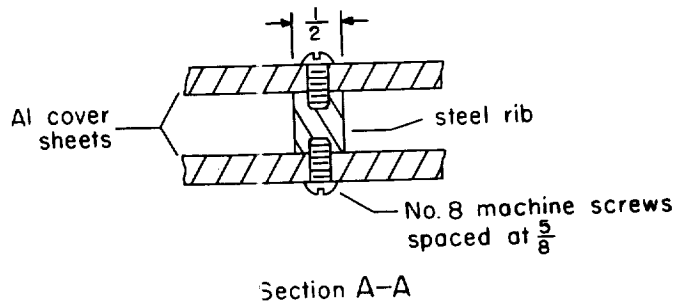
Figure 8.- Variation of $\omega/\omega_{r,T}$ with $\omega_{c,1}/\omega_{r,T}$ for antisymmetrical modes.

Detail A

|←10→|

$\frac{1}{2}$ steel rib

A   A

40

r=250

L-1444

140

$1\frac{1}{4}$

$2\frac{1}{2}$

$\frac{7}{8}$

$\frac{1}{8}$ Rivets
spaced at $\frac{1}{2}$

$\frac{1}{4}$ Rivets
spaced at $\frac{3}{4}$

.187

Detail A—Beam I

$\frac{1}{2}$

Al cover
sheets

steel rib

No. 8 machine screws
spaced at $\frac{5}{8}$

Section A—A

Figure 9.- Planform and nominal dimensions of example beam. All dimensions are in inches.
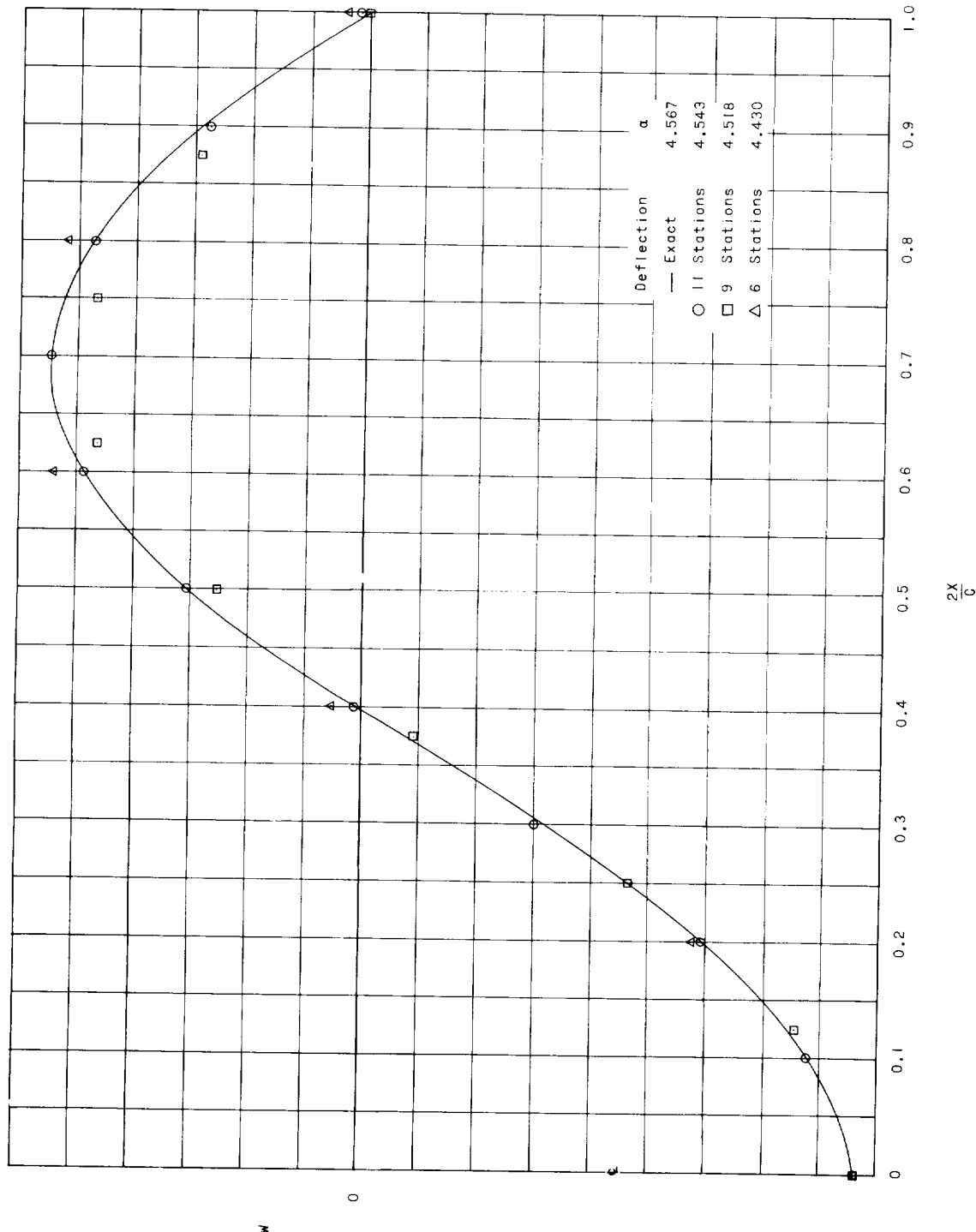
L-1444

Figure 10.- Comparison of finite-difference method with exact method for the first symmetrical mode shape. $k = 0$; $\left(\dfrac{t}{h_0}\right)^2 = 0.018$.

Deflection		α
——	Exact	4.567
○	11 Stations	4.543
□	9 Stations	4.518
△	6 Stations	4.430

$\dfrac{2x}{c}$